For publication in the Korea Australia J. of Rheology, 2001

KINEMATICS OF FILAMENT STRETCHING IN DILUTE AND CONCENTRATED POLYMER SOLUTIONS

Gareth H. McKinley[1], Octavia Brauner[1] and Minwu Yao[2]
[1]Massachusetts Institute of Technology, Cambridge, MA 02139
[2]Goodyear Technical Research Center, Akron, Ohio, USA

Abstract

The development of filament stretching extensional rheometers over the past decade has enabled the systematic measurement of the transient extensional stress growth in dilute and semi-dilute polymer solutions. The strain-hardening in the extensional viscosity of dilute solutions overwhelms the perturbative effects of capillarity, inertia & gravity and the kinematics of the extensional deformation become increasingly homogeneous at large strains. This permits the development of a robust open-loop control algorithm for rapidly realizing a deformation with constant stretch history that is desired for extensional rheometry. For entangled fluids such as concentrated solutions and melts the situation is less well defined since the material functions are governed by the molecular weight between entanglements, and the fluids therefore show much less pronounced strain-hardening in transient elongation. We use experiments with semi-dilute/entangled and concentrated/entangled monodisperse polystyrene solutions coupled with time-dependent numerical computations using nonlinear viscoelastic constitutive equations such as the Giesekus model in order to show that an open-loop control strategy is still viable for such fluids. Multiple iterations using a successive substitution may be necessary, however, in order to obtain the true transient extensional viscosity material function. At large strains and high extension rates the extension of fluid filaments in both dilute and concentrated polymer solutions is limited by the onset of purely elastic instabilities which result in 'necking' or 'peeling' of the elongating column. The mode of instability is demonstrated to be a sensitive function of the magnitude of the strain-hardening in the fluid sample. In entangled solutions of linear polymers the observed transition from necking instability to peeling instability observed at high strain rates (of order of the reciprocal of the Rouse time for the fluid) is directly connected to the cross-over from a reptative mechanism of tube orientation to one of chain extension.

1. Introduction

In a plenary presentation at the XIth International Congress in 1992, Ken Walters surveyed some of the recent developments in extensional rheometry of polymer solutions (Walters, 1992). He concluded that experimental results up to that time were 'a disappointment'; and he noted that further international co-operation and input from non-Newtonian fluid dynamics would play important roles in tackling the challenges that still lay ahead in this area of rheology. Subsequent publications have focused on the key role of controlling the fluid kinematics. The review of James & Walters (1993) surveys the difficulties inherent with devices such as opposed jet rheometers and contraction geometries. The residence time and the total strain in the region of strong extension is limited and the path of a typical fluid element does not provide a motion with constant stretch history. It is thus difficult to define an unambiguous or device-independent material function (Petrie, 1995). In the past 10 years the situation has improved dramatically with the advent of filament stretching devices (Tirtaatmadja & Sridhar, 1993). These devices have been developed and optimized for probing the extensional rheometry of 'mobile' polymer solutions; *i.e.* those that are not viscous enough to be tested in commercial devices such as the Rheometrics Melt Extensiometer (RME) commonly employed for polyolefins and other high viscosity melts (see e.g. Meissner & Hostetler, 1994). The diversity of fluids included in this category is very broad and incorporates dilute and concentrated polymer solutions, inks, adhesives, gels, suspensions, foodstuffs and also lower-viscosity melts such as polycarbonate, Nylon or PET.

Filament stretching devices have their genesis in the work of Matta & Tytus (1990) who suggested using a small cylindrical mass accelerating freely under gravity to stretch a small liquid bridge connecting the mass to a stationary support. Photographic analysis of the rate of decrease in filament radius can then be used to compute an extensional stress growth under the action of a constant force. In the same year, Bazilevsky *et al.* (1990) described a Liquid Filament Microrheometer that may best be summarised as a quantitative version of the 'thumb and forefinger' test we all commonly use to ascertain the 'stickiness' of a suspicious unknown material! The device imposed a rapid extensional step strain to generate an unstable 'necked' liquid bridge connecting two cylindrical disks which then evolved under the action of viscous, elastic, gravitational and capillary forces. Measuring the time rate of change in the diameter allowed material properties of the test fluid to be quantified. These techniques are examples of a field I shall refer to collectively as *filament stretching rheometry*. A detailed review of the development of these devices is given elsewhere (McKinley & Sridhar, 2001).

When viscoelastic filaments are stretched in a filament stretching device they may also exhibit elastically-driven flow instabilities that lead to complete filament failure, even before the stretching has been completed. Such instabilities have typically been described to date by heuristic rheological concepts such as 'spinnability' and 'tackiness'. At first glance, such instabilities may seem to limit the utility of filament stretching rheometers, but additional useful material information can be discerned

from careful measurements of the dynamical evolution of the force and radius during the failure event. Such tests may usefully be considered as the functional equivalent of the 'Rheotens' test of spin-line strength for melts (Wagner *et al.* 1996). Two distinctly different modes of filament failure can typically be observed depending on the extent of strain-hardening present in the fluid. In order to probe each of these we focus in the present study on the transient extensional response of two different classes of complex non-Newtonian fluids; unentangled dilute polymer solutions and concentrated/entangled polymeric fluids. Although both materials are viscoelastic, the microscopic mechanisms governing the evolution in the stress are different and these affect the strain-hardening of the material and the subsequent evolution in the kinematics of the elongating filament.

2. Filament Rheometers

A filament stretching experiment begins with the generation of a long and slender viscoelastic thread. For a slender filament, the velocity field far from the rigid endplates is essentially one-dimensional and extensional in character (Schultz, 1982). Many configurations for generating such flows have been suggested in the literature but, for rheometric purposes at least, two geometries have proved optimal:

- In a filament stretching extensional rheometer (or FISER) a nominally-exponential endplate displacement profile is imposed in order to produce an elongational flow of constant deformation rate, $\dot{\varepsilon}_0$ rather than constant tensile force, as in the original concept of Matta & Tytus. The temporal evolution in the tensile force exerted by the fluid column on the endplate and in the filament radius at the axial midplane of the filament are then measured and used to compute the transient extensional viscosity.

- By contrast, in a capillary breakup extensional rheometer – or CABER for brevity – an extensional step strain of order unity is imposed and the filament subsequently evolves under the influence of capillary pressure without further kinematic input at the boundaries. Large extensional strains can still be attained as the mid-region of the filament progressively necks down and eventually breaks. Typically the only measured quantity is the midpoint radius, $R_{mid}(t)$, of the necking filament.

Both of these experiments can be performed using the same device simply by specifying the total axial strain accumulated before the motion ceases. A typical filament stretching device developed at MIT for extensional rheology of a range of fluids is shown below:

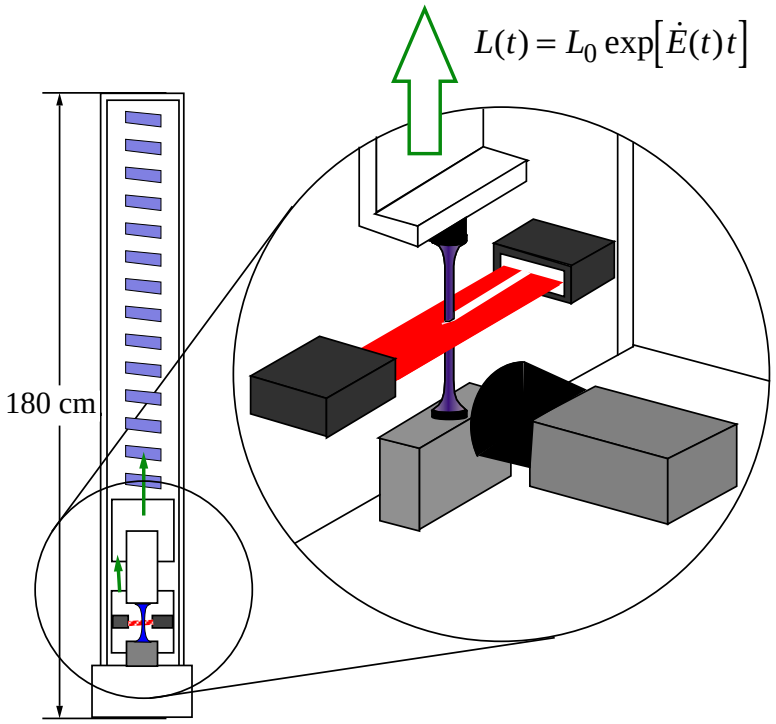

Figure 1: Schematic diagram of the components comprising a typical Filament Stretching Rheometer (FISER). By halting the motion at a small but finite strain, the capillary breakup of the thread can also be monitored.

The size of the rigid-end plates constraining the fluid can be changed over the range $0.3 \le D_0 \le 1.0$ cm and the dynamical range of the force transducer can be varied from $10^{-2} \le F \le 10^{2}$ N. A laser micrometer with a calibrated resolution of 5 μm (Anna & McKinley, 2001) measures the evolution in the midplane diameter of the filament, $D_{mid}(t)$ and a video camera provides high-resolution images of the filament profile near the end plate.

3. Kinematics of Filament Stretching Devices

In an ideal homogeneous uniaxial elongational deformation we wish to consider the effects of an irrotational flow on an initially cylindrical fluid element. This potential flow can be represented as

$$v_r = -\tfrac{1}{2}\dot{\varepsilon}_0 r; \qquad v_\theta = 0; \qquad v_z = \dot{\varepsilon}_0 z \tag{1}$$

However in experiments it is not possible to realize such a configuration. At small strains, the no-slip condition arising from the rigid end fixtures leads to a 'reverse squeeze flow'. Since the stress in a dilute polymer solution is carried primarily by the solvent for small strains, this flow can be considered analytically using a lubrication analysis (Spiegelberg *et al.* 1996) and the strain rate of material elements near the middle of the filament is found to be 50% larger than the value based on the rate of separation of the endplates; $\dot{\varepsilon}_0 = 1.5\dot{\varepsilon}_L$. At larger strains, $\varepsilon \ge 2$, simulations and experiments show that strain-hardening significantly affects the rate of evolution in the mid-filament diameter of a viscoelastic fluid.

Numerical simulations show that the principal advantage of a filament stretching experiment is that the measurements of force and midpoint radius always correspond to observations of the constitutive response of the *same* Lagrangian fluid element; *i.e*. the element located at the axial midplane of the elongating filament (Kolte et al. 1997; Yao et al. 1998a,b). This is in contrast to other techniques such as a Spinline Rheometer in which a single integrated measurement of the total tension is used to characterize the spatially unsteady kinematics experienced by material elements as they traverse the spin-line (Petrie, 1995).

The simplest approach is to impose an ideal exponential stretching deformation at the end plate of the form $L_p(t) = \exp\lfloor \dot{E}\, t \rfloor$ however this does NOT result in a homogeneous elongation of the fluid sample due to the no-slip conditions on the endplates discussed above. The instantaneous deformation rate experienced by the Lagrangian fluid element at the axial midplane can be determined in a filament rheometer in real-time using the high resolution laser micrometer which measures $R_{mid}(t)$ and using the relationship

$$\dot{\varepsilon}_{mid}(t) = \frac{-2v_r(r = R_{mid})}{R_{mid}} = \frac{-2}{R_{mid}} \frac{dR_{mid}}{dt} \tag{2}$$

The Hencky strain accumulated by the midpoint element can be found by direct integration of eq. (2) to give

$$\varepsilon = \int_0^t \dot{\varepsilon}(t')\ \mathrm{d}t' = 2\ln\left(R_0 / R_{mid}(t)\right). \tag{3}$$

This type of experiment is referred to as a Type II experiment using the nomenclature of Kolte, Szabo & Hassager (1997). However, to explore more precisely the actual constitutive response of a fluid it is necessary to decouple the kinematics from the resulting evolution in the polymeric stresses so that the appropriate constitutive equation can be directly integrated. It is thus essential to impose a <u>constant</u> rate of deformation:

$$\dot{\varepsilon}_0 = -\frac{2}{R_{mid}} \frac{\mathrm{d}\, R_{mid}(t)}{\mathrm{d}\, t} = -2 \frac{\mathrm{d}\, \ln\left(R_{mid}(t)/R_0\right)}{\mathrm{d}\, t}, \tag{4}$$

This is referred to as a Type III experiment and the goal of kinematic control in a FISER can thus be stated in the form:

Find the form of $L_p(t)$ such that $\dot{\varepsilon}_{mid}(t) = \dot{\varepsilon}_0$ for all times $t \geq 0$

The Deborah number resulting from such an experiment is constant and given by $De = \lambda \dot{\varepsilon}_0$ where λ generically denotes the longest (model-dependent) relaxation time of the test fluid. The flow is then a *motion with constant stretch history* and the constitutive equation for a representative material element can be integrated independently of solving the complete equation of motion for the entire filament.

In their groundbreaking paper, Tirtaatmadja & Sridhar (1993) used an iterative approach to finding the required endplate displacement profile, $\dot{L}_p(t)$. More recently open and closed-loop control strategies have been considered which considerably simplify the task of the experimentalist (Orr & Sridhar, 1999; Anna *et al.* 1999). Numerous experimental FISER variants have been developed, and by precisely controlling this endplate displacement profile it is now possible to reliably attain the desired kinematics. The results can be best represented on a "Master Curve" showing the evolution of the *imposed* axial strain $\varepsilon_L = \ln\left(L_p(t)/L_0\right)$ vs. the *resulting* radial Hencky strain at the midplane: $\varepsilon_{mid} = -2\ln\left(R_{mid}(t)/R_0\right)$. Very recent computational rheometry analysis shows that this approach is well-posed for a number of different constitutive models. Sample Type II calculations (ideal exponential axial stretching)are shown below in Figure 2 for the Newtonian, Oldroyd and Giesekus models. For an ideal uniaxial elongation the two strain measures are the same such that $\varepsilon_L = \varepsilon_{mid}$, whereas for the lubrication solution describing reverse squeeze flow we expect $\varepsilon_L = \frac{2}{3}\varepsilon_{mid}$.

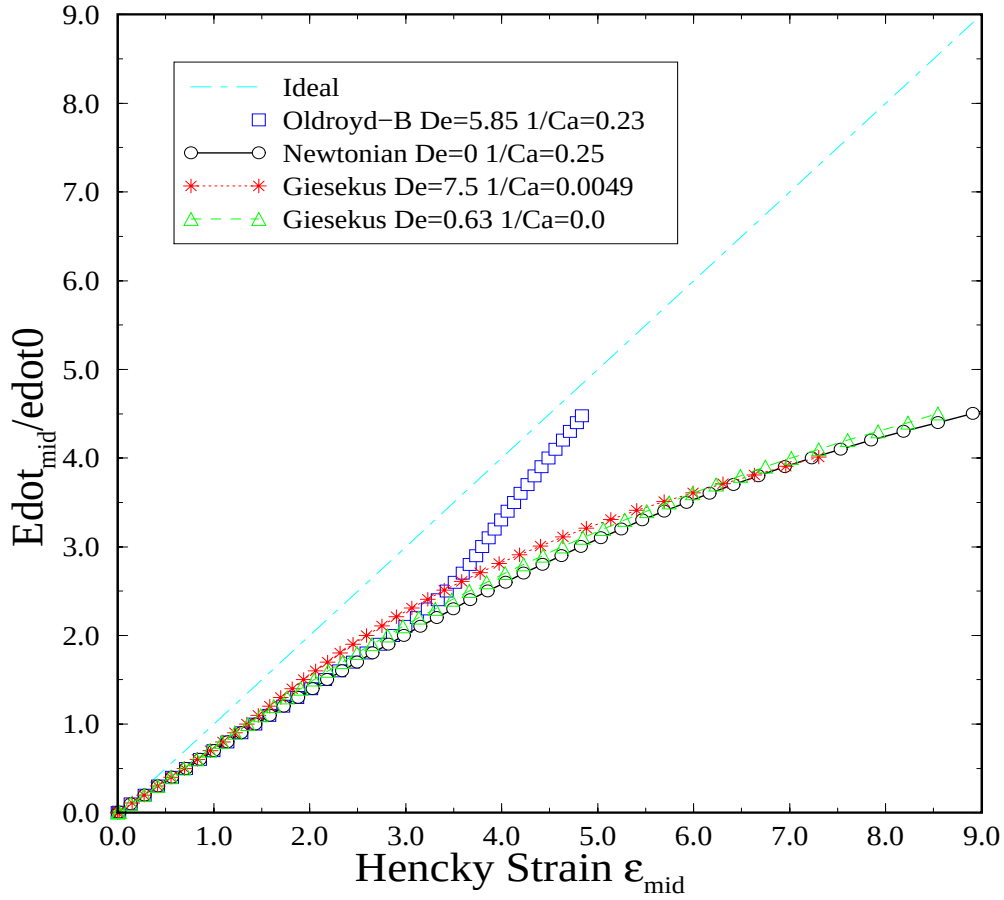

Fig..2 Master curve of axial and radial strain measures numerically computed for different constitutive models over a range of Deborah and capillary numbers.

Close inspection of Fig 2 shows that ALL viscoelastic fluid models initially follow this lubrication solution since the viscoelastic stresses are negligible at short times. At long times and larger strains, however, the different constitutive models predict very different evolution in the master curve profiles. For strongly strain-hardening fluids (e.g. the Oldroyd-B model which describes dilute polymer solutions such as ideal elastic Boger fluids) the curve eventually approaches the ideal limit corresponding to uniaxial elongation of a cylinder. However for a weakly strain hardening material (e.g. the Giesekus model which describes entangled materials such as concentrated solutions or melts) the curves progressively diverge from the ideal case. This is a result of a viscoelastic necking instability which is currently of great interest both experimentally and theoretically since it is related to concepts of melt strength and' spinnability'.

An analogous master curve is shown below for a concentrated polystyrene solution consisting of 12 wt% monodisperse polystyrene (M_w = 2x10^6 g/mol.) dissolved in TCP.

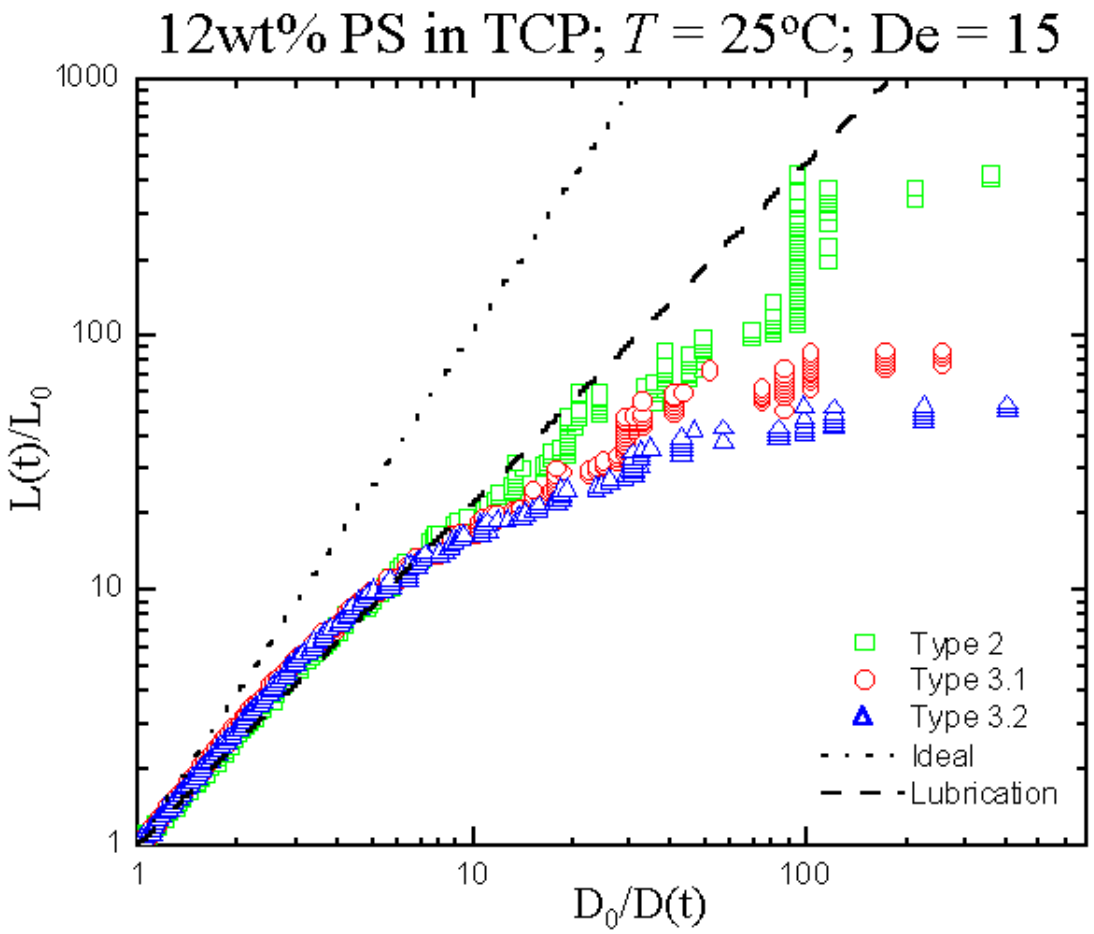

Fig. 3 Convergence of the master curve of axial and radial strain measures for 12 wt% entangled polystyrene experimentally measured in consecutive tests.

This fluid has been characterized in steady simple shear and exponential shear by Venerus and co-workers (Kahvahnd & Venerus 1994). The fluid is moderately entangled with $M_w/M_e \approx 10$ and a longest time constant that is typically denoted as a 'reptation time' or 'disengagement time' $\lambda \equiv \tau_d \approx$ 15 s. For such weakly strain-hardening fluids our numerical calculations and experimental tests show that it is necessary to perform multiple iterations in order to converge on a final master curve. The output $R_{mid}^{[j]}(t)$ from the *j*-th test is used in conjunction with the 'master curve' as a mapping function to provide the input data $L^{[j+1]}(t)$ for the next test. This iterative approach is initiated using a type 2 measurement with a constant imposed exponential separation of the endplates. Numerical simulations supporting the convergence of this 'successive substitution approach to open-loop control are reported elsewhere (McKinley & Yao, 2001). The successive evolution of the resulting master curve for experiments with the 12 wt% fluid is shown in figure 3. The first iteration leads to a relatively large change in the mapping function; however the iteration rapidly converges. After 3 iterations successive tests overlay each other within the experimental errors (typically ±5%) that are inherent in the measurements.

4. Experimental Results of Filament Stretching Rheometry

The experimental observables in a filament stretching experiment include the global evolution in the axial profile of the filament $R(z,t)$, the midpoint radius $R_{mid}(t)$, and the tensile force on the endplate $F_z(t)$. The evolution in the force is typically non-monotonic, showing an initial, solvent-dominated peak at early times, followed by strain-hardening and, possibly, a second maximum at large strains after the extensional stresses saturate and the extensional viscosity of the fluid reaches its steady-state value. A complete analysis of the appropriate force balance for the filament is given by Szabo [19]. After removing contributions from surface tension, gravity and inertia, the transient uniaxial extensional viscosity is given by

$$\eta_E^+(\dot{\varepsilon}_0,t) \equiv \frac{F_z(t)}{\pi R_{mid}(t)^2 \dot{\varepsilon}_0} \quad . \tag{5}$$

A sample force profile for a dilute polymer solution is shown below. This ideal elastic fluid is part of a homologous series studied by Anna et al. (2001) in an international 'round-robin' comparison of filament stretching devices. At short times ($\varepsilon < 2$) the stress in the fluid is carried entirely by the viscous oligomeric solvent and the filament profile is that of a concave liquid bridge (see also Yao et al. 1998a). At intermediate times ($2 \le \varepsilon \le 4$) significant strain-hardening is observed and the elastic force increases. At larger times the force goes through a maximum as the stress begins to saturate until ultimately the fluid undergoes an elastic instability at a critical strain $\varepsilon_{crit} \approx 5.1 \pm 0.1$. This peeling instability leads to a significant 'spike' in the force profile (when plotted on a linear scale rather than the usual logarithmic scale utilized in rheometry) and the onset of a symmetry breaking transition leading to

the formation of elastic fibrils (Spiegelberg & McKinley, 1997; Ferguson et al. 1998). The similarities and differences between a type 2 (specified endplate extension) and a type 3 (controlled midplane extension) test are also shown in the figure. Although the response of the two tests is qualitatively similar, the quantitative values of the force and the critical conditions for onset of instability are clearly sensitive to the entire deformation history experienced by the filament.

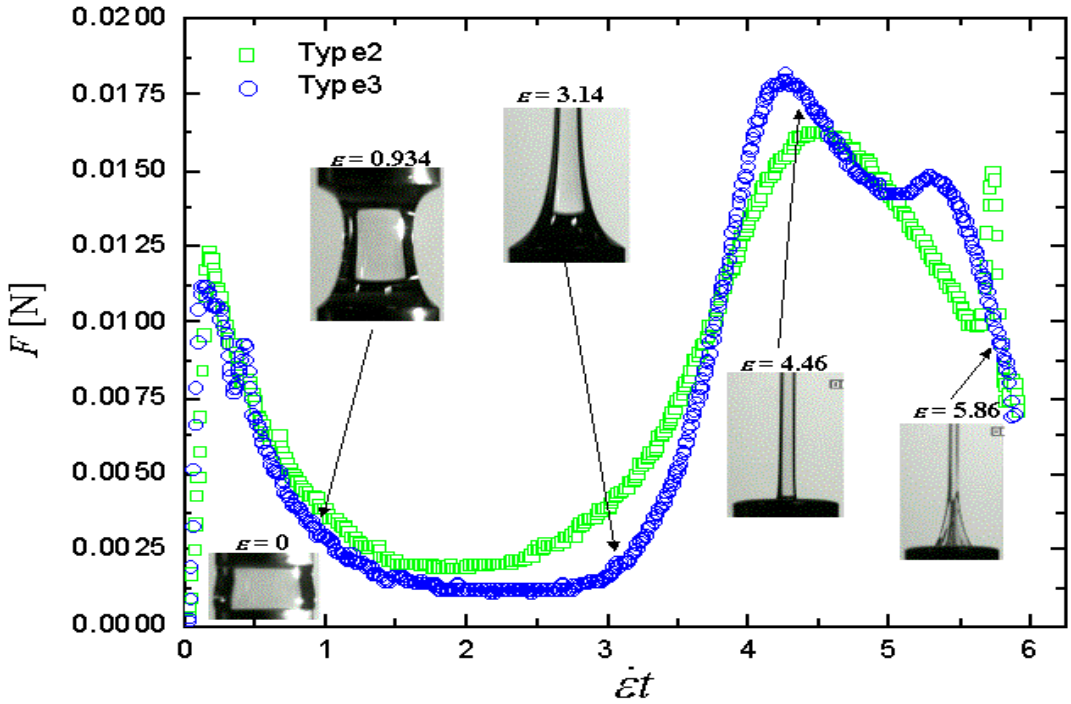

Fig. 4 Evolution in the tensile force curve and axial filament profile in Type II and Type III elongational stretching experiments for a dilute polystyrene Boger fluid.

For comparison, the evolution in the force profiles in the entangled concentrated PS solution are shown as a function of deformation rates in Figure 5. It si clear that two distinct filament elongation processes can be observed. At low deformation rates the filament forms a neck and the force passes through a single maximum; whereas at higher deformation rates the force increases dramatically and a necking instability reminiscent of that observed in the dilute solution is once again observed. Since the reported relaxation time of the fluid is τ_d = 15 s, it is clear that the transition between these two responses does not correspond to $De \approx 0.5$ and other physics must be involved.

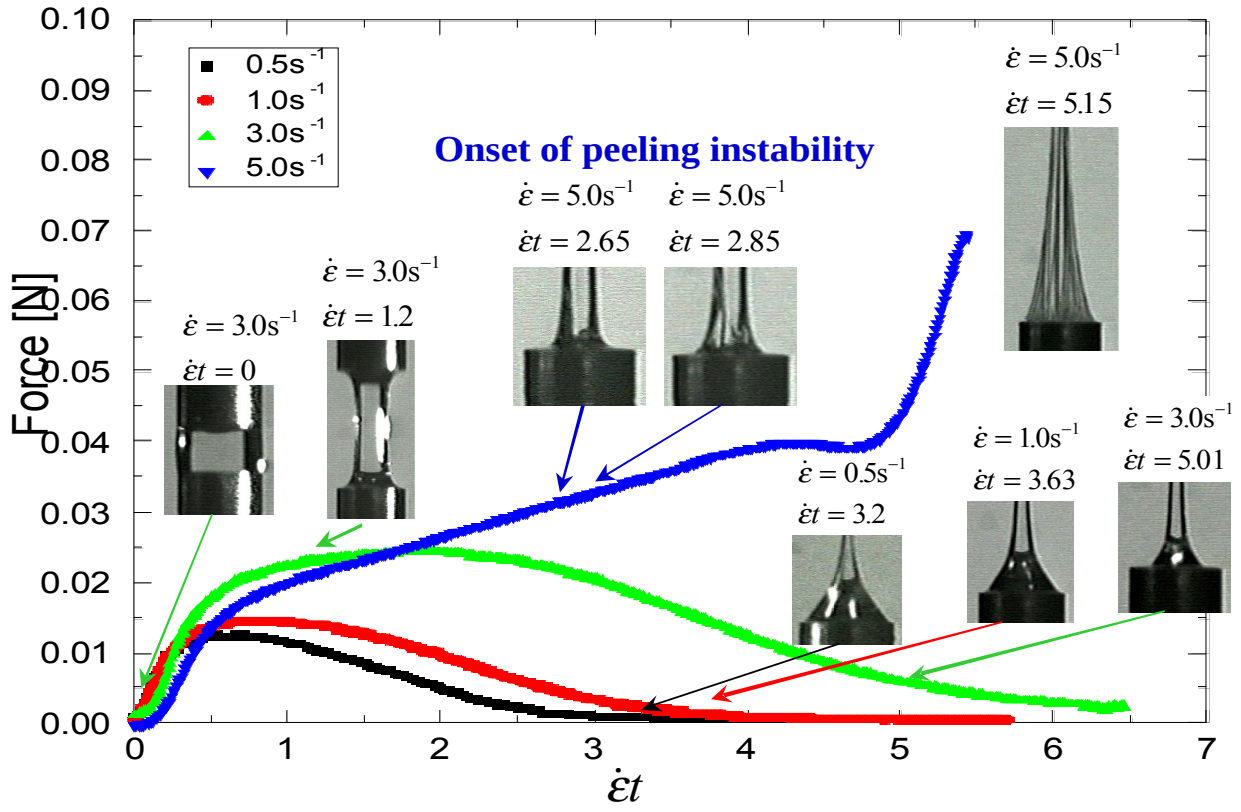

Fig. 5 Evolution in the tensile force curve and filament profile for a weakly strain-hardening entangled polystyrene fluid

In entangled solutions it is essential to recognize that there are several important characteristic polymeric time scales (Doi & Edwards, 1986), including the reptation time (typically denoted τ_d) for the tubes, the Rouse time for chain stretching (denoted τ_R) within the tube, and finally the Rouse time τ_e for a chain segment between entanglement points. Each of these relaxation processes contribute to the overall level of stress in the system; however the relative contribution of each process depends on the time scale (or deformation rate) of interest. A comprehensive theory for the linear viscoelastic properties of entangled linear chains has recently been developed which incorporates the important role of 'contour length fluctuations' into the reptation framework (Milner & McLeish, 1998). These so-called "breathing modes" lead to important differences in the linear viscoelastic predictions at intermediate frequencies $\omega \sim 1/\tau_R$ and also help account for the discrepancy between experimental observations and reptation theory predictions for the molecular weight scaling of the zero-shear-rate viscosity (Milner & McLeish, 1998). In figure 6 we show the predictions of this theory for the 12 wt% solution of PS in TCP. The number of entanglements is determined from molecular parameters for the chain and the solvent quality to be $Z \equiv M_w / M_{e,\text{soln}} \approx 15$ and the plateau modulus is $G^0_{N,so\ln} = 2.21 \times 10^3\, Pa$. The only free parameter

to be fitted is then monomer friction coefficient ζ_0 or, equivalently, the Rouse time constant τ_e of an entangled segment . The Rouse time constant for the longitudinal diffusion of the chain is given by $\tau_R = Z^2\tau_e$ and the reptation or disengagement time is $\tau_d \approx 3Z^3\left(1-1/\sqrt{Z}\right)^2$. The agreement between the experimental data for both $G'(\omega)$ & $G''(\omega)$ and the Milner-McLeish theory is extremely good over a wide range of frequencies.

The material response in a strong deformation such as an elongational flow can be understood in terms of this complex spectrum. At low deformation rates $\tau_d{}^{-1} \le \dot{\varepsilon}_0 < \tau_R{}^{-1}$ the fluid is only weakly strain-hardening as the confining tube is oriented with the flow but the chain itself remains relaxed at close to its equilibrium length within the tube. In this case the force in the filament passes through a maximum and ultimately decays at large strains as the radius at the midplane exponentially decays. In this case the filament does not show a peeling instability but instead a 'necking' instability close to the midplane. This necking instability has also been considered theoretically (Ide & White 1976; Olagunju, 1999) and numerically (Yao et al. 2000). However, at higher deformation rates $\frac{1}{2}\tau_R{}^{-1} \le \dot{\varepsilon}_0$ constitutive models such as the Doi-Edwards-Marrucci-Grizutti (DEMG) model show that chain stretching can occur and, consequently, extensive strain-hardening in the elongational viscosity is observed. This results in the endplate peeling observed at the imposed strain rate of $\dot{\varepsilon}_0$=5 s^{-1} in Figure 5 above. From the critical conditions for onset of peeling, we can thus estimate that $\tau_R \approx 0.13 \pm 0.03$ s. It is also worth noticing that because of the lower extensibility of the entangled chains ($L^2_{\text{entangled}} \sim M_e$ cf. $L^2_{dilute} \sim M_w$) the onset of peeling occurs at a significantly lower Hencky strain.

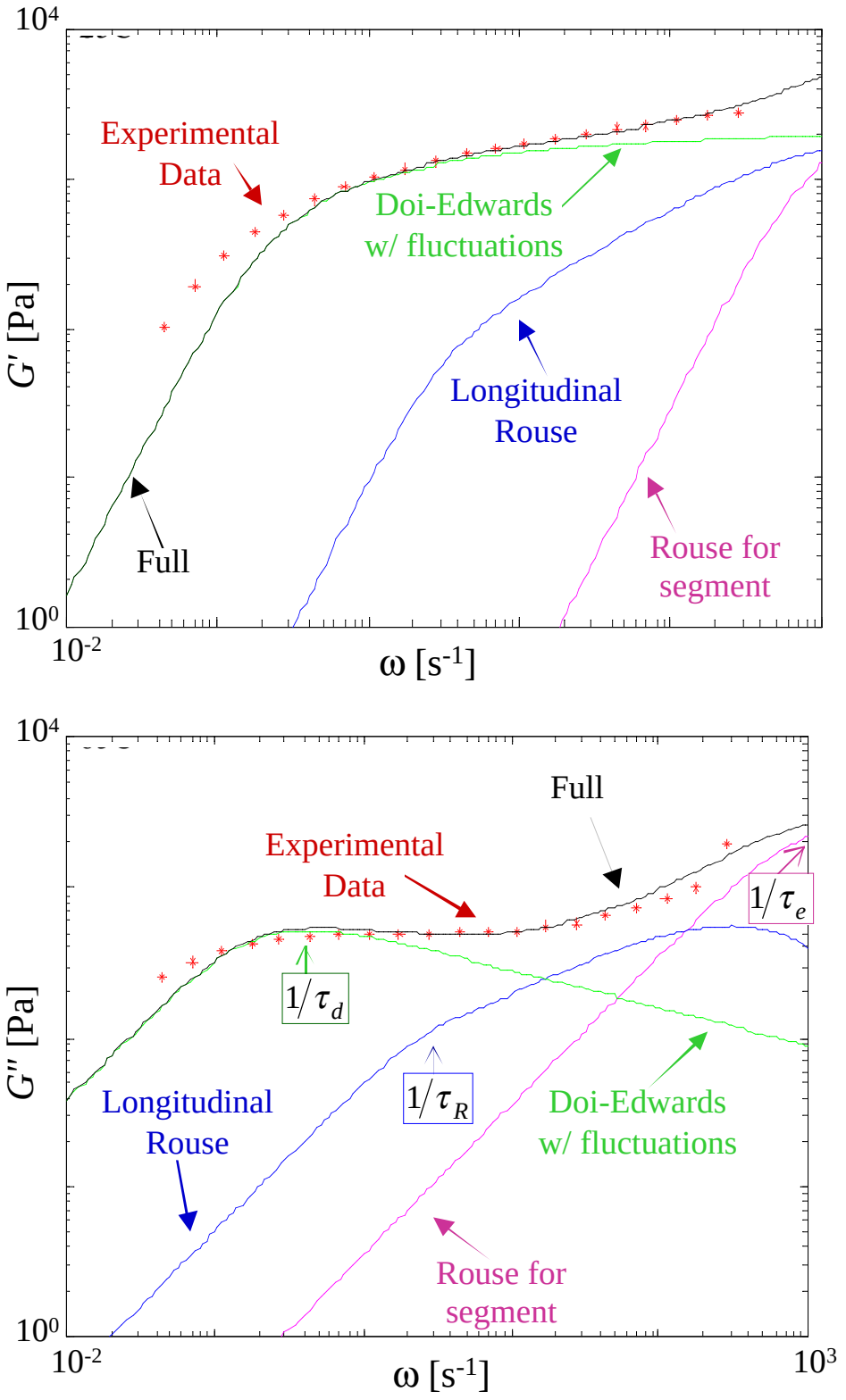

Figure 6. Linear viscoelastic properties of the 12wt% concentrated entangled polystyrene solution showing (a) elastic modulus and contribution of each mode of relaxation; (b) loss modulus showing location of the principal relaxation time for each mode of stress relaxation.

Despite the onset of the necking instability at low strain rates and the elastic peeling instability at large strain-rates, filament stretching devices can still be used to extract the transient elongational viscosity function $\eta_E^+(\dot{\varepsilon}_0, t)$ provided that the master curve methodology described above is utilized to realize an ideal 'Type III' master curve. The evolution in the Trouton ratio for the concentrated polymer solution is shown below in Figure 7 over a range of stretch rates.

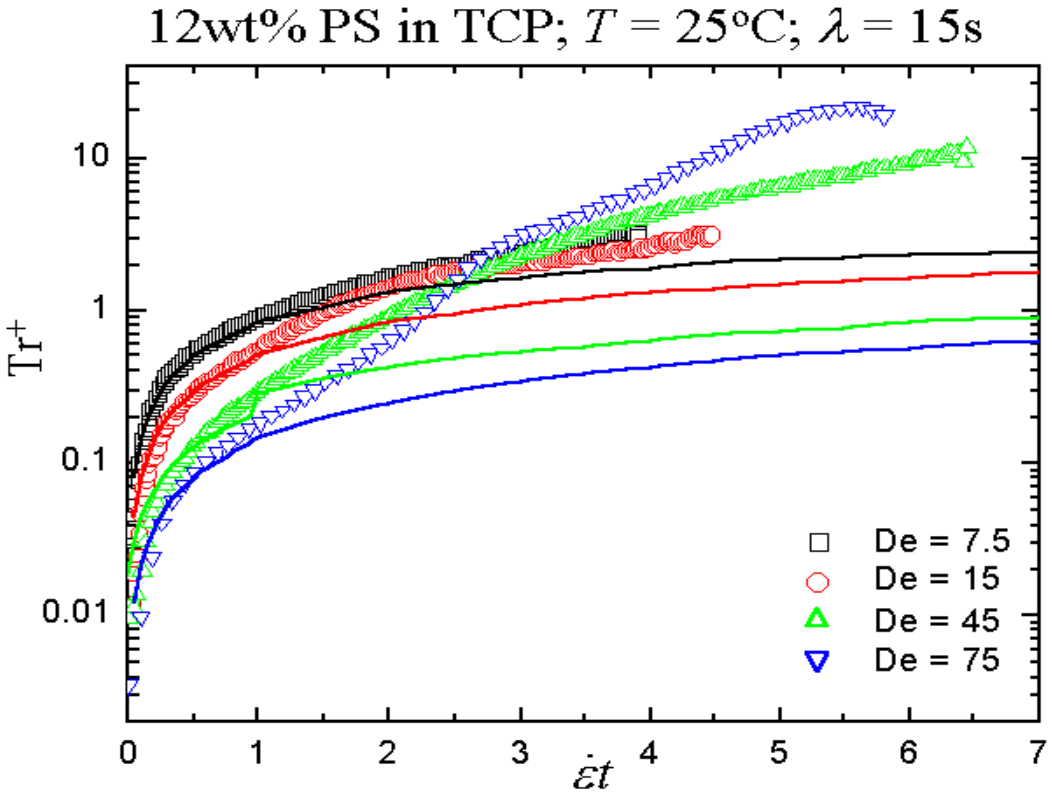

Fig. 7 Transient extensional viscosity for the 12 wt% entangled PS fluid as a function of stretch rate. The Deborah number is defined in terms of the reptation time, $\tau_d = 15$ s.

The solid lines in Figure 7 show the results expected from linear viscoelastic theory which gives

$$Tr^+ \equiv \frac{\eta_E^+}{\eta_0} = \frac{1}{\eta_0}\sum_{i=1}^{n} 3\eta_j\left(1-\exp(-t/\lambda_j)\right) = \frac{1}{\eta_0}\sum_{i=1}^{n} 3\eta_j\left(1-\exp\left(-\dot{\varepsilon}_0\, t/(\lambda_j\dot{\varepsilon}_0)\right)\right) \qquad (6)$$

where we have indicated explicitly in the last expression that since it is typical to plot the Trouton ratio vs. the total Hencky strain $\varepsilon = \dot{\varepsilon}_0 t$, the linear viscoelastic predictions do vary with $\dot{\varepsilon}_0$. We have used the 9 mode discrete spectrum of relaxation modes $\{\eta_j, \lambda_j\}$ reported by Venerus and co-workers with no

adjustments. At small strains it is clear that we can recover the linear viscoelastic envelope before strain-hardening develops at higher strains and strain rates. The onset of chain stretching at higher De (corresponding to $De_R \approx \tau_d \dot{\varepsilon}_0 / (3Z) \sim O(1)$ can be clearly identified. As we have noted above, the maximum Trouton ratio is much smaller than observed in dilute solutions due to the reduced extensibility of the entangled segments.

7. Conclusions

The number of materials tested in filament stretching devices continues to expand and now includes a number of dilute and semi-dilute 'Boger' fluids, entangled polymer solutions and melts and also liquid crystalline solutions. It seems fair to say that filament stretching results now form a standard component of the suite of tests used to characterise many polymer solutions and other complex fluids. For entangled polymeric materials (e.g. semi-dilute and concentrated entangled solutions and polymer melts), the filament stretching device provides a chance to probe the different regimes of molecular response (e.g. tube orientation, chain stretching) that are predicted from molecular-based theory. Present work focuses on extending such studies to other polymer topologies such as star polymers and branched polymer systems.

Much work remains to be done in theoretically understanding the onset of the elastic instabilities that occur at large strains; however additional information about the extensional rheology of the material is encoded in these responses and deserves detailed analysis. Future advances in this area will no doubt result from the same elements that have so benefited the first decade of filament stretching rheometry; a strong interplay between experiment, numerical simulation and kinetic theory, together with a spirit of international collaboration.

Acknowledgments

This work has been supported in part by grants from the Lord Corporation, DuPont Educational Aid Foundation, and NASA through grant NCC3-610.

BIBLIOGRAPHY

S.L. Anna and G.H. McKinley, *J. Rheol.* (2001) 45 115-138.

S.L. Anna, C.B. Rogers and G.H. McKinley, *J. Non-Newt. Fluid. Mech.* (1999) 87 307-335.

S.L. Anna, G.H. McKinley, D.A. Nguyen, T. Sridhar, S.J. Muller, J. Huang and D.F. James, *J. Rheol.* (to appear Jan/Feb 2001).

A.V. Bazilevsky, V.M. Entov and A.N. Rozhkov, in "*Third European Rheology Conference*", (*Ed.* D.R. Oliver) Elsevier Applied Science, (1990), 41-43.

M. Doi, and S.F. Edwards, The Theory of Polymer Dynamics, OUP, Oxford, 1986.

J. Ferguson, B. Reilly and N. Granville, *Polymer* (1997) 38 795-800

Ide, Y. and White, J.L., *J. Appl. Polym. Sci.*, **20**, (1976), 2511-2531.

M.I. Kolte, H.K. Rasmussen and O. Hassager, *Rheol. Acta* (1997) 36 285-302.

J.E. Matta and R.P. Tytus, *J. Non-Newtonian Fluid Mech.* (1990) 35 215-229.

G.H. McKinley, and T. Sridhar, *Ann Rev. Fluid Mech* (2001) 34 in press.

J. Meissner and J. Hostettler, *Rheol. Acta* (1994) 33 1-21.

S.T. Milner, and T.C.B McLeish, *Phys Rev Lett.* (1998) 42 81-110.

D. O. Olagunju, *J. Non-Newt. Fluid Mech.*, **87**(1), (1999), 27-46.

N.V. Orr and T. Sridhar, *J. Non-Newt. Fluid Mech.* (1999) 82 203-222.

C.J.S. Petrie, *Rheol. Acta* (1995) 34 12-26.

W.W. Schultz, *J. Rheol.* (1982) 26 331-345.

S.H. Spiegelberg, D.C. Ables and G.H. McKinley, *J. Non-Newt. Fluid Mech.* (1996) 64 229-267.

S.H. Spiegelberg and G.H. McKinley, *J. Non-Newt. Fluid Mech.* (1996) 67 49-76.

P. Szabo, *Rheol. Acta* (1997) 36 277-284.

V. Tirtaatmadja and T. Sridhar, *J. Rheol.* (1993) 37 1081-1102.

M.H. Wagner, V. Schulze and A. Göttfert, *Polym. Eng. Sci.* (1996) 36 925-935.

K. Walters, in "*Theoretical and Applied Rheology*", Vol. 1, (Ed. P. Moldenaers and R. Keunings) Elsevier, Brussels (1992), 16-23.

M. Yao and G.H. McKinley, *J. Non-Newt. Fluid Mech.* (1998) 74 47-88.

M. Yao, G.H. McKinley and B. Debbaut, *J. Non-Newt. Fluid Mech.* (1998) 79 469-501.

M. Yao and G. H. McKinley, to appear in *Proc. PRCRIII* (Vancouver, CA), Aug. 2001.